Applied Catalysis B: Environmental 203 (2017) 899–909

Contents lists available at ScienceDirect

Applied Catalysis B: Environmental

journal homepage: www.elsevier.com/locate/apcatb

Parametric study and kinetic testing for ethanol steam reforming

Matteo Compagnoni, Antonio Tripodi, Ilenia Rossetti*

Dip. Chimica, Università degli Studi di Milano, INSTM Unit Milano Università and CNR-ISTM, via C. Golgi 19, 20133 Milan, Italy

ARTICLE INFO

Article history:
Received 5 July 2016
Received in revised form 28 October 2016
Accepted 1 November 2016
Available online 2 November 2016

Keywords:
Ethanol steam reforming
Kinetic testing
Reaction mechanism
Ni-based catalysts
Hydrogen production

ABSTRACT

An experimental kinetic investigation has been carried out for ethanol steam reforming (ESR). The selected catalyst was a K-promoted Ni/ZrO_2 sample prepared by flame pyrolysis, which revealed particularly active and stable for this application based on previous investigation. Ethanol conversion, selectivity to the main possible byproducts (methane, ethylene and acetaldehyde), hydrogen productivity and the CO/CO_2 ratio, as a measure of the contribution of the water gas shift reaction, were correlated to the temperature, water/ethanol ratio and space velocity in a central composite experimental design. The parametric dependence of the reaction outcomes helped the qualitative assessment of the best operating conditions and suggested hypotheses on the reaction mechanism. A more quantitative parametric analysis was carried out by multivariate analysis.

Particularly dramatic experimental conditions have been adopted in order to highlight the formation and further evolution of possibly critical intermediates, such as ethylene and acetaldehyde. To keep ethanol and intermediates conversion below 100% at sufficiently high temperature to guarantee coke-free operation, the space velocity and feed dilution were increased. This will enable drawing a kinetic model accounting for the detailed evolution of such species.

An increase of temperature did not adequately improved H_2 selectivity, whereas the water/ethanol ratio was an effective parameter to push H_2 productivity. The reforming reactions of ethanol and of acetaldehyde/ethylene byproducts were dependent on the three parameters (kinetically controlled), whereas the CO/CO_2 ration was substantially independent on the space velocity, indicating that the water gas shift reaction reached an equilibrium value.

1. Introduction

Ethanol steam reforming (ESR) has been widely studied in the last decade as a promising mean for the production of hydrogen from renewable sources [1–4]. Ni-based catalysts were often adopted due to sufficiently high activity, acceptable cost and availability for possible scale up. Some attempts of process intensification were also proposed, since ESR can be effectively carried out at significantly lower temperature than methane steam reforming (MSR), thus allowing lower heat input to the process [5–8]. However, in spite of the full ethanol conversion achieved at temperature as low as 400–500 °C, catalyst deactivation by coking is a major issue at such low temperature, due to the concomitance of different coke formation processes and inefficient carbon gasification by steam. Coke may form through parallel routes. One is hydrocarbon decomposition and carbide accumulation, which is significant predominantly at high reaction temperature. By contrast, exothermal C formation pathways include the Bouduard reaction (CO disproportion). Ethanol dehydration to ethylene can also occur at moderate temperature, favoured over surface acidic sites, which also promote ethylene polymerisation. Both these mechanisms can be related to catalyst coking at low operating temperature. Carbon may also cover the metal active sites (encapsulating coke) or accumulate subsurface with generation of carbon nanotubes. This latter route is particularly favoured over bigger Ni particles and/or poorly interacting with the support [5,9–12].

Possibly, unreformed byproducts may also be present in the products mixture when operating at low reaction temperature, in general decreasing hydrogen yield. The most common ones are methane, which is insufficiently converted below 600 °C, acetaldehyde and ethylene. The latter can be a coke precursor, while acetaldehyde formation is often correlated to metal particles coverage by encapsulating coke. Therefore, understanding the mechanism of formation and conversion of these compounds under different reaction conditions is compulsory for process design, development and simulation, but detailed kinetic data and models including these intermediates are substantially lacking.

* Corresponding author.
E-mail address: ilenia.rossetti@unimi.it (I. Rossetti).

http://dx.doi.org/10.1016/j.apcatb.2016.11.002
0926-3373/

Some important investigations have been carried out to unravel ESR reaction mechanism and to provide kinetic parameters [13–25].

A simple Langmuir Hinshelwood kinetic model for a Ru-based catalyst was proposed by Vaidya et al. [16], considering the main reactions only to account for ethanol conversion and hydrogen yield, without details on intermediates formation and reforming. More detailed surface mechanism was proposed by Sahoo et al. [17] for a Co-based sample, accounting for ethanol decomposition to form methane, but MSR, acetaldehyde and ethylene formation/reforming were not considered. Mas and coworkers [18,20] focused on kinetics of supported Ni catalysts, including MSR, dry reforming of methane and surface reactions for ethanol decomposition. However, also in this they did not focus on acetaldehyde or ethylene which, as previously underlined, may be important byproducts. Again, an Eley Rideal kinetic model has been selected by Patel et al. [21], accounting for methane formation, but neglecting other possible byproducts.

A commercial Ni-based MSR catalyst has been proposed for ESR under different conditions and compared with a supported Rh catalyst, evidencing operating windows to lower selectivity to CO (500 °C) and to improve resistance to coking (700 °C) [26]. However, kinetic parameters and reaction networks are not made explicit. A Ni/Al_2O_3 catalyst was also studied by Wu et al., summarising the literature kinetic models and proposing a Langmuir Hinshelwood one on their own data [14]. Furthermore, a simple power rate law approach has been compared with a Langmuir Hinshelwood one for an Ir-based catalyst, accounting for part of the interesting intermediates and products and showing that models with at least 2 distinct adsorption sites (corresponding respectively to metal and oxide mediated reactions) may be needed in some cases [25]. Rival models have been also compared to kinetic data for the steam reforming of crude ethanol solutions, *i.e.* a diluted ethanol solution including lactic acid and glycerol [13]. Finally, kinetic data without detailed modelling have been reported for a Ni/Mg-Al-O catalyst [15].

Insights on the actual reaction mechanism and the formation of relevant intermediates and byproducts have been provided by theoretical, ab initio, DFT computations in addition to more traditional experimental works. Wang et al. [27] accounted for ethoxide formation followed by dehydration to ethylene on Ni, addressing the importance of C—H and O—H abstraction. A similar evolution of the adsorbed ethanol was confirmed by Christiansen et al. [28] in the framework of competitive ethylene and diethylether production. In both these works, a qualitative distinction was made between Ni, Rh, Co, Ir on one side and Au, Ag, Cu on the other. Similar studies on Pt by Sutton et al. [29], while giving different results for ethoxide stability, also established the importance of acetaldehyde as a key intermediate (by itself or via its direct dehydrogenation product CH_3-C = 0). They reported similar activation barriers for C—C breaking and confirmed the importance of C—H cleavage as the likely rate determining steps. The fundamental agreement between different calculations is valuable, since they were performed with different software packages. The same authors extended their work, making a comprehensive screening of elementary reaction steps on different metals [30], stating a firmer rationale behind both experimental and theoretical findings, among which i) the different stabilities of ethoxide on different metals (notably, Pt and Pd on one side and Ni, Co on the other) and ii) the importance of AcH as intermediate for the ESR process on oxo-philic metals such as Ni.

The explanations given in the reviewed works concerning the C—O and O—H bond-breaking may be, unfortunately, less relevant for our purposes, since the cited calculations are focused only on the active metal while the importance of the catalyst supports (mostly oxides) in these reactions is well established on experimental ground.

However, theoretical DFT calculations have proved useful beyond the elucidation of the C2 adsorbates evolution, since they help to clarify the eventual phase of the ESR process, *i.e.* the equilibration between C1 byproducts (CO, CO_2 and CH_4). Catapan et al. [31] found, for example, that different H_2O contents in the reagents, the presence of different structural features in the Ni clusters and the mobilisation of adsorbed O* (clearly expected on supports as our ZrO_2, though treated differently in the DFT calculation cited) can route the WGS reaction through different pathways, which may help to understand the complex kinetic behaviour observed for this reaction, apparently not under thermodynamic equilibrium.

It clearly appears that fundamental studies on the reaction mechanism firmly deal with the fate of C2 intermediates, which also exploit a great practical relevance as byproducts. However, kinetic studies usually do not provide experimental data on the evolution of these intermediates/byproducts as a function of experimental conditions.

Therefore, we decided to undergo a systematic kinetic investigation on one of our best performing catalysts, which was produced by flame pyrolysis and was constituted by 10 wt% Ni/ZrO_2, promoted by 9 wt% K_2O [32]. ZrO_2 has been proposed as support by some authors, though its surface acidity should be better controlled by the addition of basic promoters as in the present case [1,33–41]. This sample led to good catalytic performance at low temperature and satisfactory resistance to deactivation by coking and sintering during a previous investigation. Therefore in this work we tested its performance while varying operating temperature, space velocity (contact time) and water/ethanol molar ratio. We particularly selected very stressing conditions to limit ethanol conversion and favouring the formation of the mentioned, possibly critical and underinvestigated byproducts, such as ethylene, acetaldehyde and methane. The variables space was investigated according to a central composite experimental design. Besides producing a full set of experimental data for further kinetic modelling, free to use for the reader, the parametric dependence of catalyst performance on single and multiple parameters has been addressed both qualitatively and quantitatively through statistical analysis, focusing not only on the main reaction products, but also on important intermediates (ethylene and acetaldehyde). Monitoring such species and their evolution under variable reaction conditions is helpful for the future development of a sound kinetic model and to understand their possible role on catalyst deactivation.

2. Experimental

2.1. Catalyst preparation and characterisation

The catalyst has been prepared by flame pyrolysis (FP), as described elsewhere [32]. The sample was constituted by Ni 10 wt%, supported over ZrO_2 doped with K_2O 9 wt%. $Ni(CH_3COO)_2$ $4H_2O$ (Aldrich, pur. >98%), $Zr(CH_3COO)_4$ (Aldrich, pur. >99%) and $K(CH_3COO)$ (Aldrich, pur. >99%), were dissolved in propionic acid (Aldrich, pur. > 97%) and added with the same volume of o-xylene (Aldrich, pur. > 97%). The clear solution was injected through a syringe pump into a flame pyrolysis home made burner, extensively described elsewhere [42–45]. The liquid feeding rate was 2.2 mL/min and the O_2 flowrate through the nozzle was 5 L/min, with a pressure drop of 0.7 bar across the burner.

Details on the physical-chemical properties of the material and preliminary activity testing in comparison with rival materials, doped with different alkali/alkali earth promoters, can be found elsewhere [32]. Briefly, the K-doped catalyst was prepared by FP, selected as a scalable and one-pot synthetic method rather new for this application, which can lead to peculiar catalyst properties. Its surface area was 25 m^2/g, it was constituted by rather uniform

nanoparticles (*ca*. 30 nm). Preliminary activity results showed that full ethanol conversion can be achieved even at 400 °C with the present catalyst, which thus proved very active for this application. Very CO/CO_2 ratio was achieved by doping with K with respect to the undoped sample, indicating the promotion also of the water gas shift reaction. This parameter is fundamental to limit the further treatment of reformate gas if the aim is the production of pure hydrogen or reformate with very low CO concentration. K_2O acted mainly as chemical or electronic promoter rather than a textural one. It decreased surface acidity, but it also affected Ni redox properties, crystalline phase and led to very strong metal-support interactions. It showed the lowest coking rate even after prolonged use at much lower temperature than the present ones (*i.e.* at 300 °C) and no appreciable deactivation nor coking at temperature higher than 500 °C.

2.2. Activity testing plant

The activity tests were carried out in a bench scale micropilot plant, constituted by an Incoloy800 downflow continuous tubular reactor (40 cm in length, 0.9 cm inner diameter), heated by an electric oven whose temperature was controlled by an Eurotherm mod. 3204 TIC. The oven isothermal portion was 9 cm in length and the catalyst bed (max 5 cm) was placed in the middle. Fig. 1 shows the scheme of the plant.

The catalyst (0.15-0.25 mm particle size) was weighted in different amounts according to the desired space velocity for each test and diluted 1:3 (vol/vol) with SiC of the same size. This dilution was selected in order to limit the cold spot across the reactor and to achieve a maximum $\Delta T = \pm 1.5$ °C in the catalyst bed. The void space of the reactor was filled with quartz beads, *ca.* 1 mm in size. The catalyst was activated in 50 cm^3/min of a 20% H_2/N_2 gas mixture, while heating by 10 °C/min up to 800 °C for 1 h.

Activity testing was carried out by feeding a liquid mixture of $H_2O + CH_3CH_2OH$ by means of a Hitachi, mod. L7100, HPLC pump, added with 56 cm^3/min of N_2, used as internal standard, and 274 cm^3/min of He. Gas flow rate was controlled by Brooks mod.SLA5850S mass flowmeters. Both the liquid flow rate and reactants ratio were varied during kinetic testing according to a predetermined design of experiments (DoE). Preliminary testing was carried out to set the maximum liquid flow rate sustainable in order to keep all the mixture outflowing the reactor in gas/vapour phase even at the lowest conversion.

The activity tests were carried out at atmospheric pressure and the analysis of the out-flowing gas was carried out by an Agilent 7890 gas chromatograph, properly equipped and calibrated to quantify ethanol, water, hydrogen, carbon mono- and di-oxide, acetaldehyde, ethylene, ethane, acetone, diethylether and methane. Repeated analyses of the effluent gas were carried out and the data have been elaborated as better detailed elsewhere [40].

2.3. Kinetic testing

All the experimental testing plan was conducted over the same catalyst batch by varying 3 parameters: temperature (T), gas hourly space velocity (GHSV) and the water/ethanol feeding ratio, according to the scheme in Table 1 and Fig. 2.

At first some explorative tests were carried out to identify the optimal conditions to carry out kinetic testing and to identify the central point of the plan. Testing was not carried out at temperature lower than 550 °C to avoid possible coking (especially at low water/ethanol ratio). The maximum catalyst amount was 132 mg in order to achieve sufficiently high GHSV according to the calibration range of the HPLC pump. The flow rate of liquid feed has been fixed at 0.038 mL/min. The dilution with SiC was done in different ratio in order to keep the same bed length for every test. The minimum dilution (higher catalyst amount) was selected in order to keep the cold spot controlled within 1.5 °C, whereas the maximum dilution was selected in order to avoid bypass effects [46]. The absence of external mass transfer limitations was checked by comparing two tests carried out at the same GHSV but different catalyst amount. The effect of particle size on the catalyst efficacy factor was also checked by comparing the results obtained with different particle size (0.05–0.125 mm). The results were equal within the experimental error.

Table 1
Scheme of the kinetic testing experimental plan. W/E = water/ethanol ratio.

Code	T (°C)	GHSV (h^{-1})	W/E (mol/mol)	Catalyst mass (mg)
−2	550	25,000	3.0	132
−1	575	50,000	3.5	66
0	600	75,000	4.0	44
+1	625	100,000	4.5	33
+2	650	125,000	5.0	26

Table 2
Detail of the kinetic testing conditions. W/E = water/ethanol ratio.

Code	T (°C)	GHSV (h^{-1})	W/E (mol/mol)
0/0/0 (central point)	600	75,000	4.0
1/0/0	625	75,000	4.0
2/0/0	650	75,000	4.0
−1/0/0	575	75,000	4.0
−2/0/0	550	75,000	4.0
0/1/0	600	100,000	4.0
0/2/0	600	125,000	4.0
0/−1/0	600	50,000	4.0
0/−2/0	600	25,000	4.0
0/0/1	600	75,000	4.5
0/0/2	600	75,000	5.0
0/0/−1	600	75,000	3.5
0/0/−2	600	75,000	3.0
1/1/1	625	100000	4.5
−1/1/1	575	100000	4.5
1/1/−1	625	100,000	3.5
−1/1/−1	575	100,000	3.5
−1/−1/−1	575	50,000	3.5
−1/−1/1	575	50,000	4.5
1/−1/−1	625	50,000	3.5
1/−1/1	625	50,000	4.5

After every change of experimental condition the system was equilibrated for 1 h. The tests were carried out according to the list in Table 2. Testing was performed randomly on the same sample, except for the variation of GHSV, which was done by changing catalyst loading in the reactor. Repeated analyses were carried out to average the results. The central point (code 0/0/0, Table 2) was repeated randomly to check for repeatability.

3. Results and discussion

The full results of kinetic tests are reported in Supporting informations (Tables S1-S5). The results were expressed in terms of ethanol conversion and selectivity to products. Hydrogen productivity is also reported, normalised per catalyst mass. The CO/CO_2 ratio was used as an indicator of the contribution of the WGS reaction.

The variables were tuned in the selected operating range in order to limit ethanol conversion and to highlight the formation of interesting byproducts, to make hypotheses on the reaction mechanism. However, due to the very high activity of the selected sample, in order to operate in a coke free region (T > 550 °C) [47], the GHSV was increased. This induced some experimental problems when operating at fixed catalyst amount. Indeed, at very high liquid feeding rate, especially at high W/E ratio, water condensation at reactor outlet was observed. In order to avoid this problem we preferred

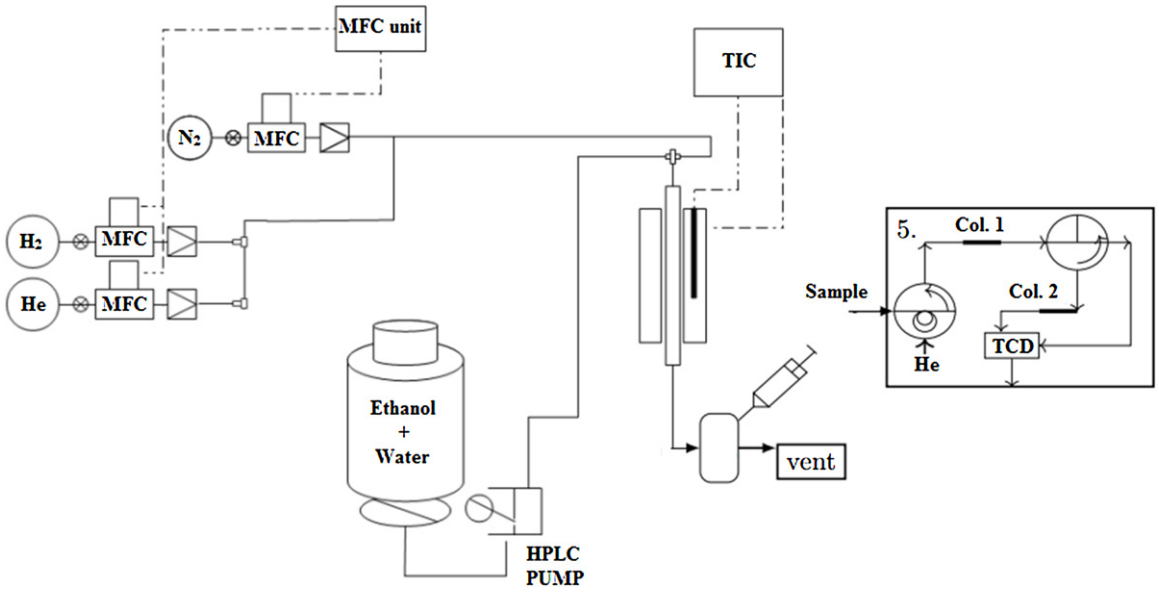

Fig. 1. Experimental plant used for the activity tests.

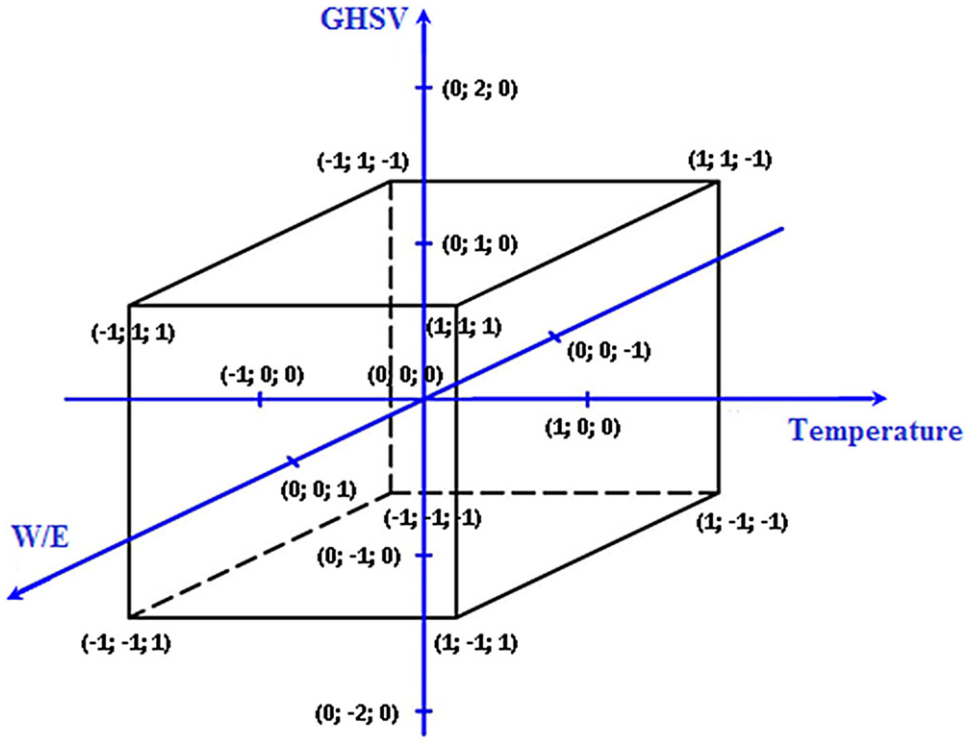

Fig. 2. Scheme of the experimental testing plan.

to keep liquid flow rate fixed, with the additional advantage of a constant fluid dynamic regime in the reactor. GHSV was therefore varied by loading different catalysts amount.

No significant coke accumulation over the catalyst was observed in the selected temperature range and W/E ratio.

3.1. *Effect of W/E ratio*

This parameter was not deeply investigated in literature although its role is crucial. In this work the W/E feeding ratio was varied starting from the lowest boundary corresponding to the stoichiometric value. Overstoichiometric mixtures are commonly used in demonstrative steam reforming units in order to push forward the WGS reaction by shifting the equilibrium conversion. Moreover, this enhances the coke gasification by water and consequently the catalyst stability, key point in an industrial view [47,48]. However the higher is the W/E ratio the higher are the operating costs due to a less energy-efficient plant as a result of increased utility costs to vaporize the feed [23] if internal energy recovery is not allowed.

Poorly concentrated bioethanol has been recently proposed as a less expensive feedstock for steam reforming [23,49]. Indeed, *ca.* 50 vol% ethanol can be obtained with relatively inexpensive purification strategies and may be conveniently used for this application without further purification.

Experimental data showed that the increase of W/E ratio induced an increase of ethanol conversion. This was in line with the simulation results obtained by us in a previous work on a demonstrative plant [23] and with the literature [50]. However, the conversion parameter is worthless without considering selectivity to by-products. Selectivity to C_2 byproducts decreased with the increasing of W/E ratio, suggesting the promotion of the reforming reaction for all the C_2 compounds. By contrast, a less remarkable effect was observed on methane selectivity, which was mainly affected by the other parameters. This point is very interesting and suggests that ethanol and acetaldehyde decomposition routes (Eq. (3) and (5)) are the main methane production paths rather than the methanation reactions starting from CO and CO_2 (Eq. (4), reversed, and (8)). This is reasonable being these reactions exothermic and not favoured thermodynamically at temperature higher than 500 °C [51], and is also in line with the findings of Wang et al. [25] about the prevalence of reforming over dehydrogenation at higher water ratios.

The CO/CO_2 ratio, decreasing with increasing the W/E feeding ratio, confirmed as expected the beneficial effect of this parameter on the WGS reaction. As a consequence of all these considerations, H_2 selectivity and productivity increased with W/E (Tables S1, S4, S5, Fig. 3). Therefore, the use of diluted ethanol (high W/E ratios) is an effective way to enhance the hydrogen yield.

Considering the possible pathways leading to the formation and conversion of all the byproducts, it can be observed that all the conversion paths for methane, ethylene and acetaldehyde can be favoured by water addition, whereas only the formation of ethylene can be inhibited by the increase of water partial pressure, consistently with reaction (1).

$$CH_3CH_2OH \rightarrow CH_2CH_2 + H_2O \quad (1)$$

$$CH_2CH_2 + 2H_2O \rightarrow 2CO + 3H_2 \quad (2)$$

$$CH_3CH_2OH \rightarrow CO + H_2 + CH_4 \quad (3)$$

$$CH_4 + H_2O \leftrightarrows CO + 3H_2 \quad (4)$$

$$CH_3CH_2OH \rightarrow CH_3CHO + H_2 \quad (5)$$

$$CH_3CHO \rightarrow CH_4 + CO \quad (6)$$

$$CH_3CHO + H_2O \rightarrow 2CO + 3H_2 \quad (7)$$

$$CO_2 + 4H_2 \leftrightarrows CH_4 + 2H_2O \quad (8)$$

$$CO + H_2O \leftrightarrows CO_2 + H_2 \quad (9)$$

From a mechanicistic point of view, the overall reforming process is based on a carbon-carbon splitting stage followed by the reversible processes (4)–(8) and water-gas shift (9). Moreover, the fact that the metal can activate C—C and C—H bonds, while —OH and —H transfers require the acid/basic sites of the supporting oxide, explains the coexistence of ethylene and acetaldehyde paths (selected by the support rather than by the metal) and the high conversion rates obtained with bare oxides [52], which are still able to dehydrogenate ethanol: the final state of the products depends then on the relative rate of C—C scission compared to that of the water-assisted CO and CH_4 reforming. Though it has been pointed out that high water fractions can decrease the *instantaneous* conversion rate due to competitive adsorption [15], this does not modify the *steady state balance* of the above reactions at sufficient catalyst loads.

3.2. Effect of reaction temperature

Temperature was changed from 550 °C to 650 °C. These conditions were milder with respect to those to be applied for the methane steam reforming (700–900 °C) [53] because of the easier reformation of an oxygenated substrate such as ethanol. The

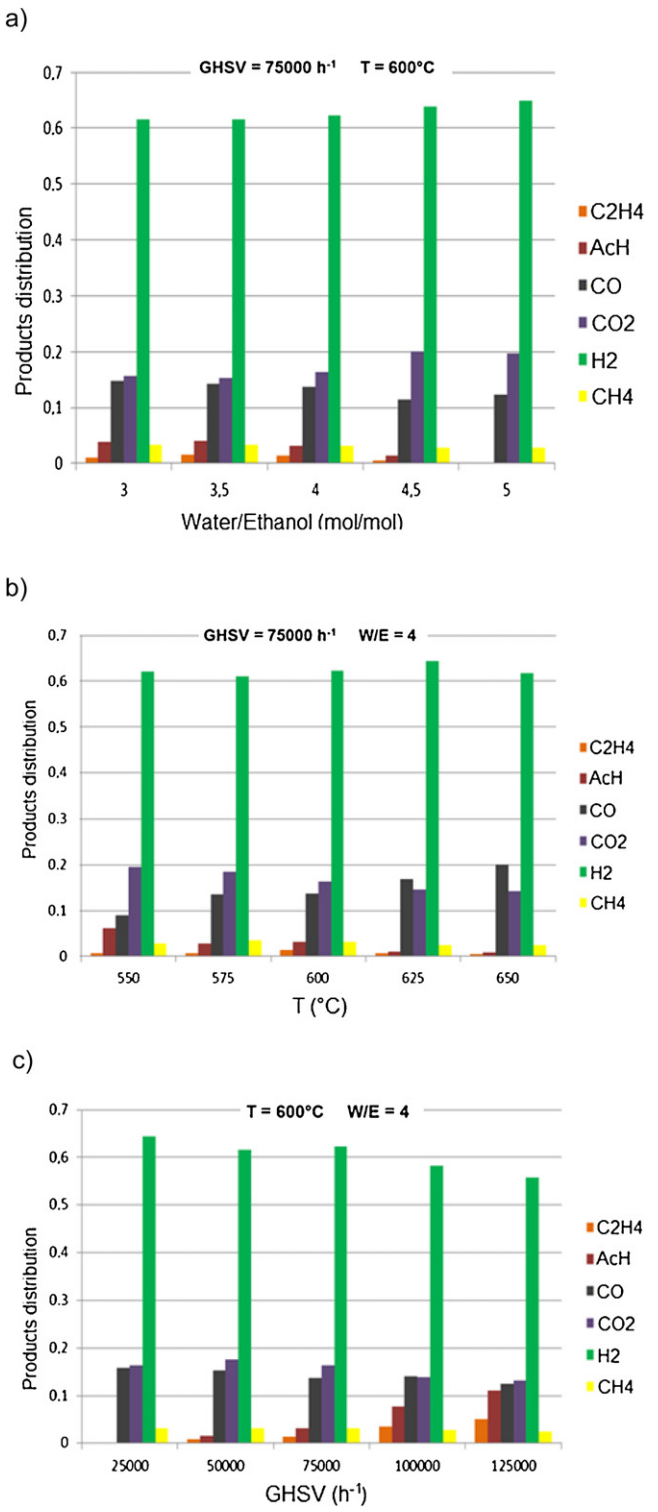

Fig. 3. Products distribution as mole fraction vs. a) W/E ratio; b) temperature; c) GHSV.

increase of temperature as expected induced an increase of ethanol conversion because of the endothermic nature of the reaction and for kinetic reasons. Also the reforming reactions of ethylene and acetaldehyde were favoured, but the methane steam reforming reaction was still insufficiently promoted, so that methane remained the primary H-containing by-product (Table S2, Fig. 3b). The exothermal WGS reaction was instead unfavoured, leading to higher CO concentration with increasing temperature (Fig. 4a).

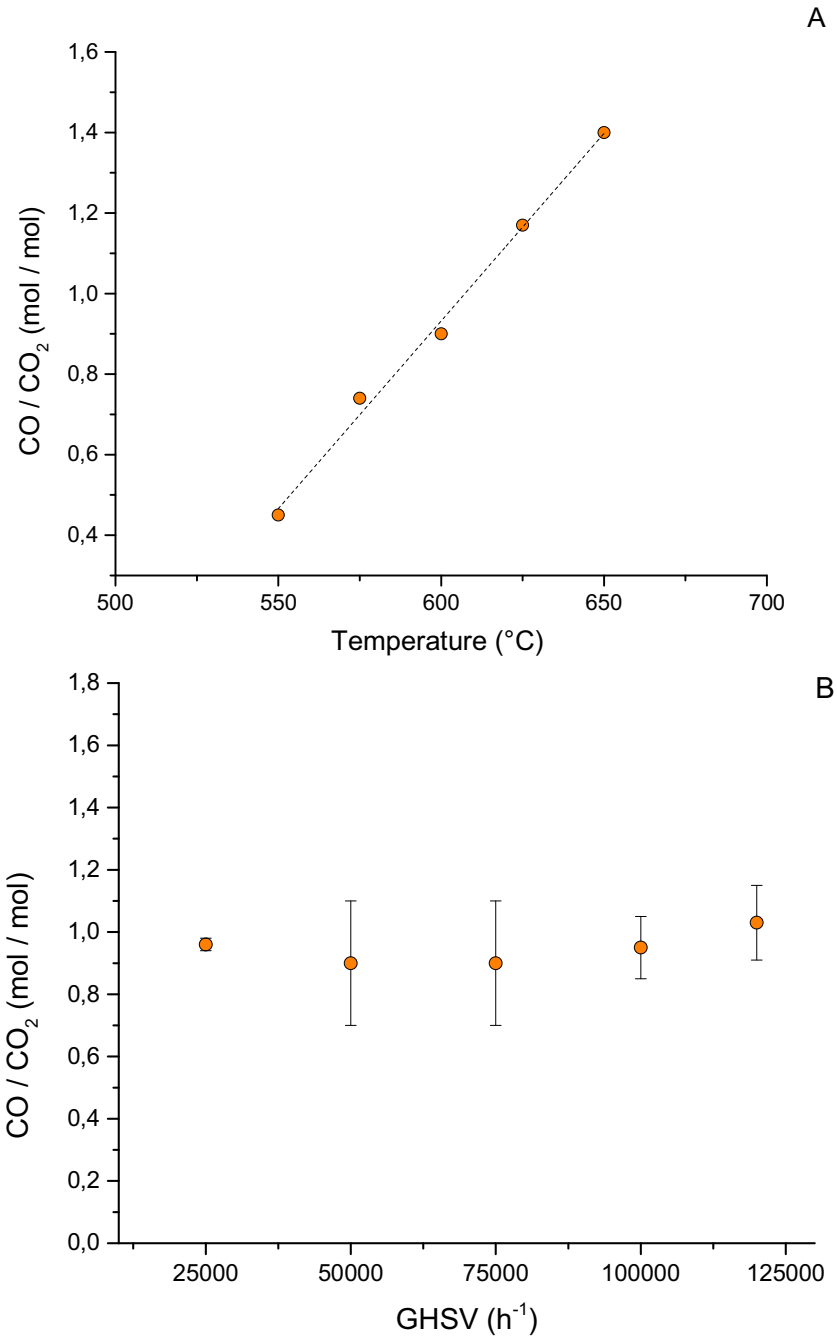

Fig. 4. Trend of CO/CO_2 ratio considering: a) different temperatures at the same space velocity (GHSV = 75,000 h^{-1}) and water/ethanol ratio (W/E = 4); b) different space velocity at the same temperature (T = 600 °C) and water/ethanol ratio (W/E = 4).

As a consequence, an increase of temperature led to decreasing selectivity to CO_2 and increasing to CO due to unfavourable WGS equilibrium. This would depress H_2 selectivity. However, increasing temperature favoured the conversion of the C_2 byproducts, which increased H_2 production. As a sum, the H_2 selectivity remained rather constant with increasing temperature due to the influence of these contradictory factors.

Song and co-workers studied the temperature effect on the reaction network using temperature-programmed reaction and isotopic labelling techniques [19]. W/E ratio equal to 8 and GHSV of 5000 h^{-1} were used, obtaining similar product distribution trend using different catalysts (Co/ZrO_2 and Co/CeO_2). The significant discrepancy with this work was the presence of acetone, observed in a range between 450 °C–550 °C, considering moreover only the acetaldehyde as starting substrate with a water/acetaldehyde ratio equal to 10. This path was confirmed by the formation mechanism of acetone, which is mainly due to acetaldehyde condensation [50] or by reaction of acetaldehyde with adsorbed methyl groups [54].

A very straightforward combination of DFT, microkinetic modelling and experimental results has been reported [30], accounting for methane and acetaldehyde formation at low temperature on a Pt-based catalyst. In particular, the initial dehydrogenation of ethanol (α C—H abstraction) was found to be the rate determining step because of the much lower concentration of adsorbed ethanol relative to CH_x species. The explanation given for the positive effect of high temperature was related to the increase of efficiency of this dehydrogenation step instead of the OH-involving ones (water-gas shift and methane reforming were not taken into account), but the

overall prediction was still in clear accordance with our results where the concentration of these compounds decrease drastically with increasing temperature.

3.3. Effect of GHSV

Correlation between reaction network and space velocity is a fundamental point for reactor sizing and for a clear explanation of the product profiles through the length of the reactor. As aforementioned, the change of GHSV was here accomplished by varying the catalyst mass. The increase of space velocity (decreasing contact time) brought about as expected a decrease of ethanol conversion, accompanied by less effective reforming of all the C_2 byproducts except methane. Consequently, H_2 productivity decreased of about 15% with respect to its highest value with increasing GHSV (Fig. 3c), while a concomitant increase of acetaldehyde and ethylene selectivity was detected (up to 29% and 13%, respectively), witnessing the progressive lack of metallic sites referred to the ethanol mole fed. This aspect was confirmed by Frusteri et al. [55] by varying the GHSV (5000–40,000 h^{-1} referred to the ethanol flow rate) on a Ni/CeO_2 catalyst.

Furthermore, the increase of selectivity to acetaldehyde and ethylene with increasing space velocity confirmed them as intermediates of a consecutive reaction network. Among the byproducts, methane showed a completely different behaviour (its concentration remained roughly constant or even mildly increasing with increasing catalyst loading, Table S3), and the prevailing role of reversible equilibrium reactions once ethanol and acetaldehyde were cracked was confirmed, together with the fact that the complete elimination of CH_4 and CO cannot just rely on a simple "conversion boost" however achieved.

Broad space velocity range was also tested by Palma et al. on bimetallic $Pt\text{-}Ni/CeO_2\text{-}ZrO_2$ catalysts, although at different temperature. Full ethanol conversion and methane as only byproduct were reported at 500 °C, W/E = 3 mol/mol and 110,000 h^{-1} [56].

The selectivity trend to CO and CO_2 is more complex: both concentrations decreased with increasing GHSV due to increased concentration of C2 byproducts, from whose reforming CO and CO_2 are produced. Nevertheless, when looking at the CO/CO_2 ratio (Fig. 4b) a substantially independent value with GHSV was achieved. This indicates that under the selected reaction conditions the WGS reaction reached a steady state condition. Thus, in order to promote WGS temperature should be decreased and W/E ratio increased, independently of the value of space velocity adopted. This point is crucial from a mechanistic point of view and not well argued in literature. Reaction quotients of WGS far from the equilibrium are often ascribed to a poor activity of nickel based materials, neglecting the role played by the oxide supports.

In order to deepen the reason for the flat CO/CO_2 pattern, a thermodynamic calculation of the WGS equilibrium was performed by the stoichiometric method [57] considering in addition the methane steam reforming. In case, coke formation was added as C-consuming reaction, considering the C balance outcomes. Calculated equilibrium values (Fig. 5) for the mixture: CH_4, CO, CO_2, H_2O and H_2 show a marked difference between the obtained CO/CO_2 ratios and the thermodynamic equilibrium conditions. Our tests confirmed the instauration of a kinetically-controlled steady state (the CO/CO_2 ratio is essentially constant for any catalyst loading that assures a high ethanol conversion, but it's not the thermodynamic one calculated by considering simple equilibria). The calculation was repeated by considering methane as inert, as suggested in the literature [30]. Fig. 5 shows a substantially higher expected CO/CO_2 ratio with respect to the experimental evidence. This lets us conclude that: i) kinetic constants for WGS and methane reforming may be not much higher than that of ethanol cracking, ii) "delayed" carbon and hydrogen atoms may come into WGS balance from previously deposited coke, to be then equilibrated by water in a completely rate-controlled way, iii) hydrogenated or oxidised species, besides pure coke, may remain irreversibly adsorbed (or be released on times comparable with the length of the tests), leading to equilibrium balances appreciably different from those based on the inlet mixture composition. This conclusion is in line with Sprung et al. [58], who explained in similar way the presence of different CO concentration with respect to the calculated equilibrium.

3.4. Overall comments

The steam reforming reaction was confirmed to be the sum of different reaction pathways. The reaction was less demanding that the steam reforming of methane, with increasing ethanol conversion at increasing temperature, W/E ratio and contact time. Therefore, the use of diluted ethanol solutions seems favourable for this application. Full ethanol conversion can be easily reached over this catalyst under mild conditions and GHSV. Thus, to evidence the different intermediates and their dependence on the operating parameters, very high GHSV should be adopted.

Ethanol can be dehydrated to ethylene, which is consequently reformed. The selectivity to ethylene was effectively decreased by raising the W/E ratio and lowering GHSV, while it showed less sensitive to an increase of the operating temperature.

Acetaldehyde was produced through dehydrogenation of ethanol and further reformed or decomposed to methane and CO. All the operating parameters deeply affected its selectivity, which decreased with increasing temperature, W/E ratio and contact time.

Methane selectivity remained rather limited (always well below 10%) and showed much lower dependence on the operating conditions. This byproduct can be effectively suppressed only by adopting much higher reaction temperature and longer contact time. Furthermore, its concentration decreased rather proportionally to the increase of acetaldehyde, suggesting that methane was predominantly formed from acetaldehyde decomposition (reaction (6)). This is in accordance with the experimental results obtained by Karim et al. [59] using 10 wt% Co/ZnO at 450 °C and GHSV of 18,000 h^{-1} although they attribute the methane formation to the direct ethanol decomposition (reaction (3)). Indeed, the details of methane formation and reforming can contribute to explain also the interplay between coke formation and WGS: mechanisms based either on quantum calculated rate determining steps (rds) [60] or heuristically defined rds [58] establish a dehydrogenation chain from CH_4^* to C^* followed by a OH^* assisted CO formation, with the first stage being slower than the second; the different role assigned to OH groups in relation to CO (with respect to the different methane-CO routes traced in [30]), together with the prevalence given by these authors to reduced CH_x^* intermediates rather than formiates, may be due to the different materials studied, as this could be the reason also for the different WGS reaction quotients found respectively by Maestri et al. [60] or by Sprung et al. [58].

Also our data fit in the framework of two consequent reforming processes (first of ethanol, then of methane) and this can be explained considering: i) the relative stability of methane, ii) the kinetic relevance of the C—H breaking even respect to the C—C breaking and iii) the connection of different kinds of coke with both ethylene and methane [15].

The rather constant selectivity to CH_4 in the conditions adopted allowed to conclude that this compound is, as expected, harsher to convert in this temperature range. However, it may also be speculated a different CH_4 formation mechanism depending on the operating conditions. For instance the cracking of acetaldehyde may be favoured under some reaction conditions, methanation or ethylene hydrogenolysis under different ones.

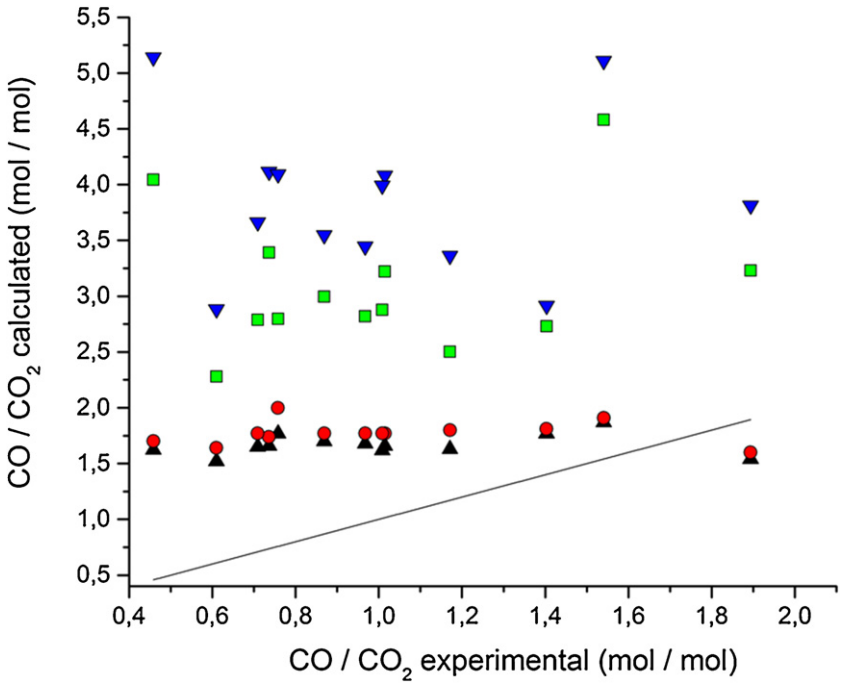

Fig. 5. Parity plot for CO/CO_2 ratios with respect to equilibrium considering (black triangles) or not considering (red circles) the coke formation. The same calculation has been repeated by considering CH_4 as inert (green squares considering coke, blue reverse triangles not considering it). (For interpretation of the references to colour in this figure legend, the reader is referred to the web version of this article.)

Finally, in order to decrease the amount of CO in the products mixture, the WGS reaction should be promoted. This reaction was substantially independent from GHSV, and the CO/CO_2 ratio varied only with temperature and W/E ratio just in parallel with the relative variation of the reaction equilibrium constant. Therefore, it can be concluded that the reaction rapidly brings the reforming products in equilibrium conditions, although not simply defined by thermodynamic calculations on simple gas phase reactions.

Overall, the parametric dependence of H_2 productivity on the operating conditions is not trivially predictable, being based on different reactions. It can be concluded that H_2 productivity can be effectively enhanced by increasing contact time, temperature and W/E ratio. The latter aspect is practically very important, opening the way to the use of very diluted bioethanol mixtures, obtainable with rather inexpensive purification methods (Fig. 6).

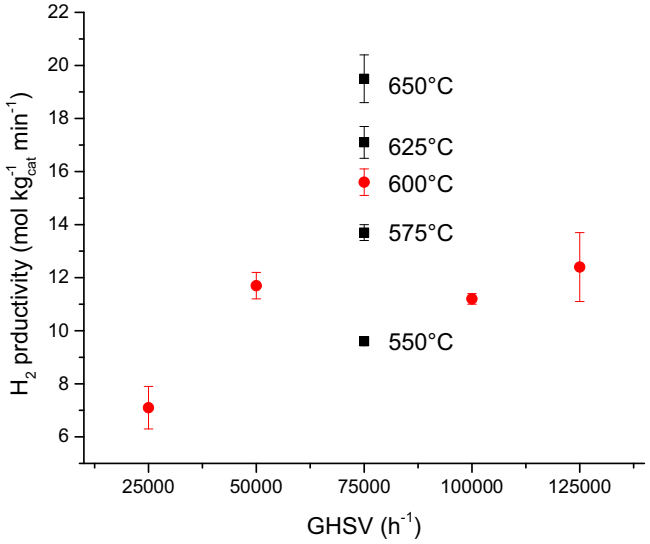

Fig. 6. Parametric dependence of H_2 productivity from operating conditions at the same W/E (equal to 4). Red dots refer to the same operating temperature (600 °C), black squares refer to the same GHSV (75,000 h^{-1}). (For interpretation of the references to colour in this figure legend, the reader is referred to the web version of this article.)

3.5. Weighting of the parametric dependence of the variables

Though sufficiently clarified by the qualitative results of the experiments, the relative role of each reaction parameter can also be quantified by linear analysis.

Following the approach of DOE analysis, we associated selected experimental outcomes (ethanol conversion, hydrogen productivity, CO/CO_2 ratio, methane and ethylene selectivity) to each point at the boundaries of the hyperspace of reaction conditions. For example, the minimum and maximum of GHSV (θ), temperature (T) and W/E ratio received a normalised value of −1 and +1, then every experiment was positioned by a coordinate triplet (θ,T,W/E) with θ={-1,1}, *etc.*

The variation $\Delta y/\Delta\theta$, $\Delta y/\Delta T$, $\Delta y/\Delta(W/E)$ was then calculated for every 'y' experimental outcome, to get a more quantitative picture of which reaction outcome was more or less affected by the variation of a given reaction variable. The lump tabulation for the analysis is summarised in Table 3, while the results of this calculation are listed in Table 4.

It was also possible to operate a full multivariate linear regression on the entire dataset. In this case, the fitted parameter is not the reaction outcome itself, but its deviation from the central value, *i.e.* the value yielded by the (0,0,0) central experiment (<y>).

The resulting linear system reads:

$$\bar{\bar{A}} \times \bar{x} = \overline{\Delta y}$$

where $\bar{\bar{A}}$ is the matrix of the j-th coordinate in the i-th experiment, while $\bar{x}$ and $\overline{\Delta y}$ are the arrays of the sought weights and of the

Table 3
Tabular representation of the experimental hyperspace with selected reaction outcomes. X: Ethanol conversion (%), other parameters are as reported in the previously reported Tables. Test IDs 3,8,13 are repeated.

ID	θ	T	W/E	X	H_2	CO/CO_2	CH_4	C_2H_4
1	0	0	−2	88	17	1.05	6.1	3.7
2	0	0	−1	90	15	0.91	5.5	5.4
3	0	0	0	92	16	0.9	6	5
4	0	0	1	97	18	0.57	6.3	2.2
5	0	0	2	100	19	0.62	7	0.6
6	0	−2	0	69	10	0.45	4.5	2.1
7	0	−1	0	84	14	0.74	6.8	2.6
8	0	0	0	92	16	0.9	6.1	5
9	0	1	0	93	17	1.17	4.8	4.3
10	0	2	0	94	19	1.4	6	2.3
11	−2	0	0	100	7	0.96	6.7	0.9
12	−1	0	0	96	12	0.9	7.4	3.3
13	0	0	0	92	16	0.9	6.1	5
14	1	0	0	81	11	0.95	3.5	9
15	2	0	0	71	12	1.03	3	13.4
16	1	1	1	83	15	1.8	4.9	2.4
17	1	−1	1	80	13	0.61	5.9	9.4
18	1	1	−1	77	14	1.6	5.8	2.8
19	1	−1	−1	71	13	0.76	4.6	6
20	−1	1	1	100	14	0.8	6.5	0.6
21	−1	1	−1	100	15	1.1	7	1.2
22	−1	−1	1	96	9	0.88	8	2.5

Table 4
Differential variations of reaction outcomes normalized to the maximal variation of reaction conditions. X: EtOH conversion (%), other parameters are as reported in the previous Tables.

	ΔX	ΔH_2	$\Delta CO/CO_2$	ΔCH_4	ΔC_2H_4
Δθ	−14.5	2.5	0.035	−1.85	6.25
ΔT	12.5	4.5	0.475	0.75	0.1
Δ(W/E)	6	1	−0.215	0.45	−1.55

Table 5
Linear regression coefficients and sum of square residues (S) extrapolated from the dataset.

	ΔX	ΔH_2	$\Delta CO/CO_2$	ΔCH_4	ΔC_2H_4
Δθ	−8.407	0.696	0.087	−1.030	2.403
ΔT	4.370	1.696	0.265	−0.014	−0.697
Δ(W/E)	2.704	0.141	−0.066	0.197	−0.459
S	638	226	0.844	13.7	114

outcome deviations for every parameter, respectively. The linear problem has been solved using the Matlab® software. The fitted coefficients Δy/Δθ, Δy/ΔT, Δy/Δ(W/E) are listed together with the sum of square residuals in Table 5. The parity plots for the regression are also presented through Fig. 7a–e.

Finally, the combined effect of more than one experimental condition can be evaluated building additional independent variables as the pair products: θ *x* T, θ *x* (W/E), T *x* (W/E), and repeating the linear regression above described with six independent variables instead of three.

To try this analysis, however, the dataset had to be reduced, as the extreme values of any variable (coded as −2,+2) are always paired to the nominal values (identically null) of the others, so to yield couple products always equal to 0. These points would have no effect on the regression and would be indistinguishable from the pivotal triplet (0,0,0), which is meaningless; so the results derived from this analysis (based on a sub-space ranging from −1 values to +1 only) cannot be directly compared to the others. The results are reported in Table 6.

While the simple DOE approach tends to overestimate the role of temperature in achieving high conversions, the full and second-order regression assign more correctly a dominant role

Table 6
Linear regression coefficients for the second-order analysis and sum of square residues (S), extrapolated from the subspace of (-1, +1) points.

	ΔX	ΔH_2	$\Delta CO/CO_2$	ΔCH_4	ΔC_2H_4
Δθ	−10.346	−0.392	0.119	−1.156	1.696
ΔT	1.854	0.608	0.263	−0.366	−1.424
Δ(W/E)	1.454	−0.792	−0.056	0.134	−0.334
ΔθΔT	1.058	0.365	0.232	0.258	−0.558
ΔθΔ(W/E)	2.808	1.615	0.040	0.033	0.767
ΔTΔ(W/E)	0.558	1.365	0.002	−0.417	−0.233
S	197	95	0.357	4.20	47.4

to the contact time. Regarding H_2 yield, temperature is identified as the leading parameter by the first two analysis, while the W/E ratio is assigned a high importance only by the 2nd order approach. Ethylene is unmistakably recognised as intermediate by all the approaches, since high positive weights are always placed upon θ. The role of the (W/E) ratio is recognised with the correct sign for ethylene (which stems for a dehydration) and for the CO/CO_2 ratio, affected by water always in a negative way.

While the second order analysis itself may be slightly less robust, it is worth to notice some interesting clues it can provide: for example, while ΔT and Δ(W/E) seem to have an equal 1st order role determining ethanol conversion, the sensibly different weights calculated for ΔθΔ(W/E) respect to ΔTΔ(W/E) help to clarify that the water mixture content is likely more important. Even more interesting are the higher weights for the couples in H_2 yield: while the (W/E) ratio itself has an unexpected negative coefficient (contrary to both the expected trends of WGS reaction and steam reforming), the high positive coefficient of the product ΔTΔ(W/E) helps to sort out the fact that the equally important temperature parameter had been varied in the opposite way with respect to the water content in at least two cases (id 17–18 and 21–22), bringing to a superposition effect (the low weight assigned to the water content in the straightforward linear regression may also be due to this masking phenomenon).

The case of methane is more complex and the failure in correctly identifying the right sign for (W/E) in all the trials comes primarily from the low variation of its selectivity. Anyway also in this case the negative sign for the ΔTΔ(W/E) combination helps to clarify

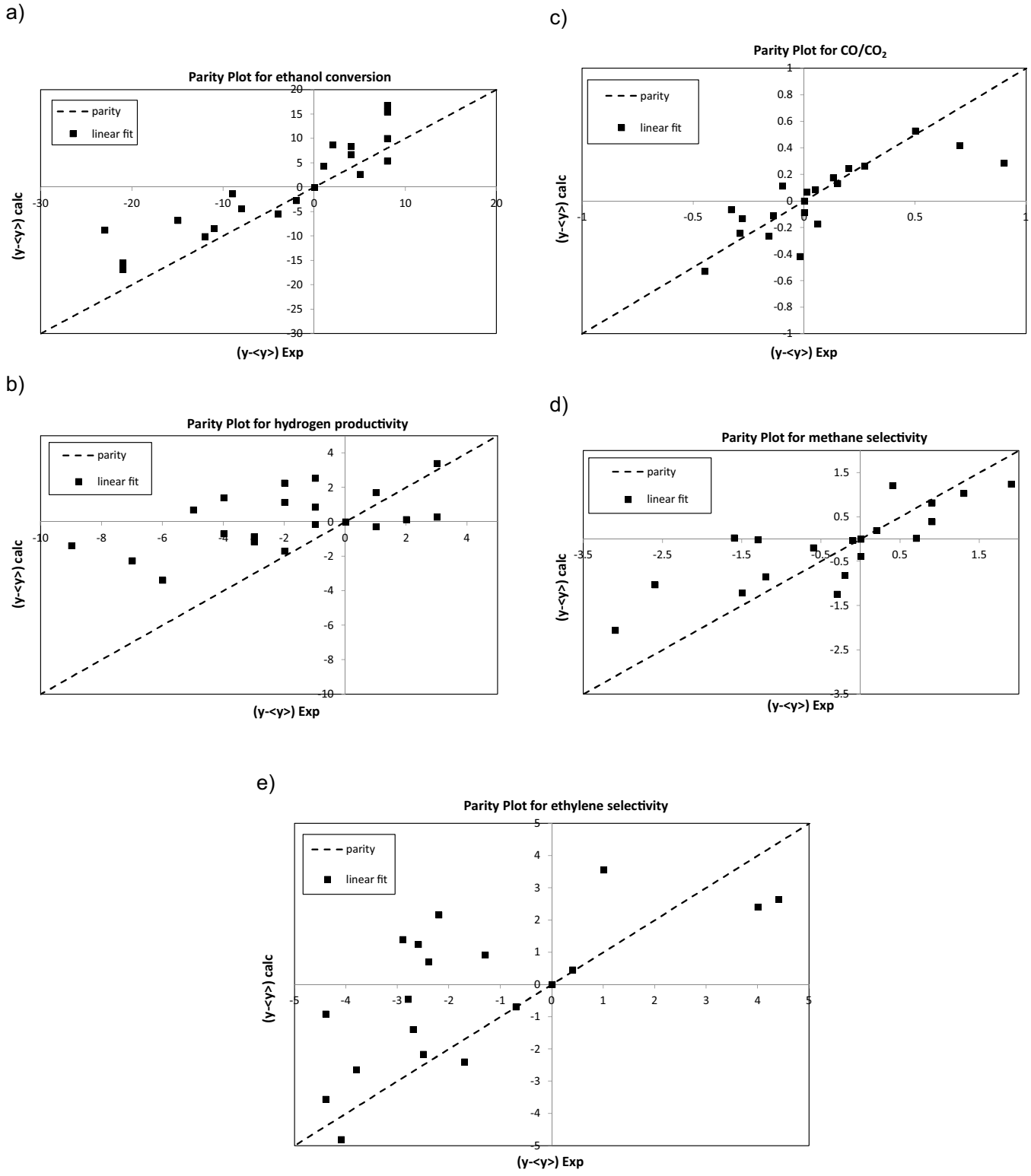

Fig. 7. Parity plot for the multivariate linear regression (first order, full dataset) of a) ethanol conversion, b) H_2 productivity, c) CO/CO_2 ratio, d) methane and e) ethylene selectivities. <y> represents the variable value for the central test (0/0/0).

that the combined effect of these parameters is indeed beneficial to methane reforming. The unexpected positive sign calculated for θ, anyway, may well be due to the fact that, as an intermediate, methane is consumed later than ethylene, besides being equilibrated by the methanation reaction.

4. Conclusions

A parametric study and kinetic testing for ethanol steam reforming has been carried out on a K-promoted Ni/ZrO_2 catalyst prepared by flame pyrolysis. We here investigated the dependence of ethanol

conversion, H_2 productivity and selectivity to different byproducts on three main variables, *i.e.* temperature, space velocity and the water/ethanol feeding ratio. We specifically selected very stressing conditions for the catalyst in order to highlight the formation of possibly critical byproducts, such as ethylene and acetaldehyde, which are not accounted for in many kinetic investigations found in the literature. A full dataset is thus available for kinetic modelling.

The water/ethanol ratio revealed a particularly interesting parameter to promote the use of diluted and less expensive bioethanol streams. In general, ethanol and C2 byproducts conversion was improved by increasing temperature, contact time and water/ethanol ratio. Methane was a minor byproduct in most cases, but showed lower dependence on most parameters. This may be related to different paths for its production and conversion, which differently depend on the operating conditions.

The reaction mechanism was discussed based on the parametric dependence of the products distribution. A more quantitative dependence of reaction outcomes on the selected variables has been provided through statistical analysis of the results. Temperature and water/ethanol ratio resulted the most important variables to define conversion and selectivity. Their combined optimisation is a straightforward route to improve H_2 productivity.

Acknowledgement

The valuable collaboration of Dr. Nicola Bagnaresi during the collection of activity and kinetic data is gratefully acknowledged.

Appendix A. Supplementary data

Supplementary data associated with this article can be found, in the online version, at http://dx.doi.org/10.1016/j.apcatb.2016.11.002.

References

[1] D. Zanchet, J.B.O. Santos, S. Damyanova, J.M.R. Gallo, J.M.C. Bueno, ACS Catal. 5 (2015) 3841–3863.
[2] J.L. Contreras, J. Salmones, J.A. Colín-Luna, L. Nuño, B. Quintana, I. Córdova, B. Zeifert, C. Tapia, G.A. Fuentes, Int. J. Hydrogen Energy 39 (2014) 18835–18853.
[3] J. Sun, Y. Wang, ACS Catal. 4 (2014) 1078–1090.
[4] J.-J. Hwang, Renew. Sustain. Energy Rev. 19 (2013) 220–229.
[5] I. Rossetti, J. Lasso, V. Nichele, M. Signoretto, E. Finocchio, G. Ramis, A. Di Michele, Appl. Catal. B Environ. 150–151 (2014) 257–267.
[6] B. Banach, A. Machocki, Appl. Catal. A Gen. 505 (2015) 173–182.
[7] M. Kourtelesis, P. Panagiotopoulou, X.E. Verykios, Catal. Today 258 (2015) 247–255.
[8] T.S. Moraes, R.C. Rabelo Neto, M.C. Ribeiro, L.V. Mattos, M. Kourtelesis, S. Ladas, X. Verykios, F.B. Noronha, Appl. Catal. B Environ. 181 (2016) 754–768.
[9] G. Ramis, I. Rossetti, E. Finocchio, M. Compagnoni, M. Signoretto, A. Di Michele, Prog. Clean Energy (2015) 695–711.
[10] I. Rossetti, J. Lasso, E. Finocchio, G. Ramis, V. Nichele, M. Signoretto, A. Di Michele, Appl. Catal. A Gen. 477 (2014) 42–53.
[11] V. Nichele, M. Signoretto, F. Pinna, E. Ghedini, M. Compagnoni, I. Rossetti, G. Cruciani, A. Di Michele, Catal. Lett. 145 (2015) 549–558.
[12] V. Nichele, M. Signoretto, F. Pinna, F. Menegazzo, I. Rossetti, G. Cruciani, G. A. Di Michele Cerrato, Appl. Catal. B Environ. 150–151 (2014) 12–20.
[13] O.A. Olafadehan, A.A. Ayoola, O.O. Akintunde, V.O. Adeniyi, J. Eng. Sci. Technol. 10 (2015) 633–653.
[14] Y.-J. Wu, J.C. Santos, P. Li, J.-G. Yu, a.F. Cunha, a.E. Rodrigues, Can. J. Chem. Eng. 92 (2014) 116–130.
[15] G. Zeng, Y. Li, U. Olsbye, Catal. Today 259 (2015) 312–322.
[16] P.D. Vaidya, a E. Rodrigues, Ind. Eng. Chem. Res. 45 (2006) 6614–6618.
[17] D.R. Sahoo, S. Vajpai, S. Patel, K.K. Pant, Chem. Eng. J. 125 (2007) 139–147.
[18] V. Mas, M.L. Bergamini, G. Baronetti, N. Amadeo, M. Laborde, Top. Catal. 51 (2008) 39–48.
[19] H. Song, L. Zhang, U.S. Ozkan, Ind. Eng. Chem. Res. 2 (2010) 8984–8989.
[20] I. Llera, V. Mas, M.L. Bergamini, M. Laborde, N. Amadeo, Chem. Eng. Sci. 71 (2012) 356–366.
[21] M. Patel, T.K. Jindal, K.K. Pant, Ind. Eng. Chem. Res. 52 (2013) 15763–15771.
[22] I. Rossetti, M. Compagnoni, M. Torli, Chem. Eng. J. 281 (2015) 1024–1035.
[23] I. Rossetti, M. Compagnoni, M. Torli, Chem. Eng. J. 281 (2015) 1036–1044.
[24] M.C. Sanchez-Sanchez, R.M.N. Yerga, D.I. Kondarides, X.E. Verykios, J.L.G. Fierro, J. Phys. Chem. A 114 (2010) 3873–3882.
[25] F. Wang, W. Cai, C. Descorme, H. Provendier, W. Shen, C. Mirodatos, Y. Schuurman, Int. J. Hydrogen Energy 39 (2014) 18005–18015.
[26] J. Vicente, J. Erena, M. Olazar, P.L. Benito, J. Bilbao, A.G. Gayubo, J. Energy Chem. 23 (2014) 639–644.
[27] J.-H. Wang, C.S. Lee, M.C. Lin, J. Phys. Chem. C 113 (2009) 6681–6688.
[28] G. Christiansen, Matthew A. Mpourmpakis, D.G. Vlachos, J. Catal. 323 (2015) 121–131.
[29] J.E. Sutton, D.G. Vlachos, Ind. Eng. Chem. Res. 54 (2015) 4213–4225.
[30] J.E. Sutton, P. Panagiotopoulou, X.E. Verykios, D.G. Vlachos, J. Phys. Chem. C 117 (2013) 4691–4706.
[31] R.C. Catapan, A.A.M. Oliveira, Y. Chen, D.G. Vlachos, J. Phys. Chem. C 116 (2012) 20281–20291.
[32] M. Compagnoni, A. Di Michele, P. Sassi, I. Rossetti, Appl. Catal. A Gen. submitted (n.d.).
[33] V. Palma, C. Ruocco, A. Ricca, Int. J. Hydrogen Energy 41 (2016) 11526–11536.
[34] M. Greluk, G. Słowik, M. Rotko, A. Machocki, Fuel 183 (2016) 518–530.
[35] Z. He, X. Wang, Catal. Today 240 (2015) 220–228.
[36] L. Guerrero, S. Castilla, M. Cobo, Quim. Nova 37 (2014) 850–856.
[37] M. Nagai, M. Akiyama, Y. Oki, J. Jpn. Pet. Inst. 55 (2012) 67–68.
[38] S. Li, M. Li, C. Zhang, S. Wang, X. Ma, J. Gong, Int. J. Hydrogen Energy 37 (2012) 2940–2949.
[39] M. Akiyama, Y. Oki, M. Nagai, Catal. Today 181 (2012) 4–13.
[40] I. Rossetti, C. Biffi, C.L. Bianchi, V. Nichele, M. Signoretto, F. Menegazzo, E. Finocchio, G. Ramis, A. Di Michele, Appl. Catal. B Environ. 117–118 (2012) 384–396.
[41] V. Nichele, M. Signoretto, F. Pinna, F. Menegazzo, I. Rossetti, G. Cruciani, G. A. Di Michele Cerrato, Appl. Catal. B Environ. 150–151 (2014) 12–20.
[42] G.L. Chiarello, I. Rossetti, L. Forni, J. Catal. 236 (2005) 251–261.
[43] G.L. Chiarello, I. Rossetti, L. Forni, P. Lopinto, G. Migliavacca, Appl. Catal. B Environ. 72 (2007) 227–232.
[44] G.L. Chiarello, I. Rossetti, L. Forni, P. Lopinto, G. Migliavacca, Appl. Catal. B Environ. 72 (2007) 218–226.
[45] G.L. Chiarello, I. Rossetti, P. Lopinto, G. Migliavacca, L. Forni, Catal. Today 117 (2006) 549–553.
[46] R.J. Berger, J. Perez-Ramìrez, F. Kapteijn, J.A. Moulijn, Chem. Eng. Sci. 57 (2002) 4921.
[47] L.V. Mattos, G. Jacobs, B.H. Davis, F.B. Noronha, Chem. Rev. 112 (2012) 4094–4123.
[48] J. Sun, Y. Wang, ACS Catal. 4 (2014) 1078–1090.
[49] I. Rossetti, J. Lasso, M. Compagnoni, G. De Guido, L. Pellegrini, Chem. Eng. Trans. 43 (2015) 229–234.
[50] T. Hou, S. Zhang, Y. Chen, D. Wang, W. Cai, Renew. Sustain. Energy Rev. 44 (2015) 132–148.
[51] G.P. Szijjártó, A. Tompos, J.L. Margitfavi, Appl. Catal. A Gen. 391 (2011) 417–426.
[52] A.N. Fatsikostas, X.E. Verykios, J. Catal. 225 (2004) 439–452.
[53] L. Pino, A. Vita, M. Laganà, V. Recupero, Appl. Catal. B Environ. 148–149 (2014) 91–105.
[54] P. Ciambelli, V. Palma, a. Ruggiero, Appl. Catal. B Environ. 96 (2010) 190–197.
[55] F. Frusteri, S. Freni, V. Chiodo, S. Donato, G. Bonura, S. Cavallaro, Int. J. Hydrogen Energy 31 (2006) 2193–2199.
[56] V. Palma, C. Ruocco, F. Castaldo, A. Ricca, D. Boettge, Int. J. Hydrogen Energy 40 (2015) 12650–12662.
[57] V. Mas, R. Kipreos, N. Amadeo, M. Laborde, Int. J. Hydrogen Energy 31 (2006) 21–28.
[58] C. Sprung, B. Arstad, U. Olsbye, ChemCatChem 6 (2014) 1969–1982.
[59] A.M. Karim, Y. Su, J. Sun, C. Yang, J.J. Strohm, D.L. King, Y. Wang, Appl. Catal. B Environ. 96 (2010) 441–448.
[60] M. Maestri, D.G. Vlachos, A. Beretta, G. Groppi, E. Tronconi, J. Catal. 259 (2008) 211–222.